

# Single-photon source with ultranarrow linewidth manipulated by coherent fields

He-bin Zhang<sup>1,\*</sup> and Gao-xiang Li<sup>1,†</sup>

<sup>1</sup>*Department of Physics, Huazhong Normal University, Wuhan 430079, China*

(Dated: December 24, 2024)

Recent works [PhysRevLett.125.170402 (2020) and PhysRevLett.125.043603 (2020)] verify that the perfect single-photon character is a global property of resonance fluorescence including all the spectral components, and then the absence of some components can spoil the single-photon character, which considerably limits the application of filtering scheme to obtain single-photon source (SPS) with subnatural linewidth. Here, we note that the linewidth of fluorescent photon is not always limited by the intrinsic linewidth of the emitter, and provide a scheme where the linewidth of the fluorescent single photon can be much smaller than the natural linewidth of emitter by manipulating external coherent fields. By simulating the response of the filter or detection setup with a bandwidth approaching and even much smaller than the natural linewidth of emitter, the realization of ultranarrow SPS can be confirmed. Besides, we demonstrate that this scheme of ultranarrow SPS can be implemented based on various real physical platforms.

The investigation on single-photon source (SPS) is of great interest since such a source is one of the cornerstones of many quantum information technologies [1, 2]. Because of perfect single-photon character, resonance fluorescence is always regarded as an important candidate for SPS, and the platforms for the implementation involve atom [3–7] and atom-like systems [8–14]. In fact, in quantum information applications such as distance quantum communication [15], optical quantum computation [1, 2, 16, 17], and solid-state quantum networks [18, 19], SPS is required to have high quality, which means that the single photons have the same frequency, polarization, narrow linewidth and so on. For instance, in optical quantum computation, the computing power is determined by the number of entangled photons. And in a promising preparation scheme of multiphoton entanglement, the maximum number of entangled photons is limited by the quality of single photons [20]. In current SPS schemes, spectral filtering is often applied to eliminate unwanted spectral components to improve the indistinguishability of the quantum sources [13, 21–23]. However, as verified by recent works [24, 25], spectral filtering may lead to the destruction of single-photon character, which means that the SPS degenerates to an ordinary source. Therefore, in simple fluorescence, the simultaneous observation of subnatural linewidth and single-photon character is considered impossible.

On the other hand, the researches on the spectral line narrowing of fluorescence by means of well-designed physical mechanisms have attracted many attentions. In general, the arising of the narrow and even ultranarrow peak in fluorescence spectrum can be attributed to the slow decay rate of a metastable state [26]. And the appearance of the metastable state originates from a variety of mechanisms, such as the modification of the reservoir [27, 28], the vacuum induced coherences [29–33], and the slow decay channel introduced by attaching a metastable state to the decaying state [34–37]. We note that these researches mainly focus on the appearance of narrow line in

fluorescence spectrum, and the narrowing spectral components only account for a fraction of fluorescence so that cannot serve as the SPS with subnatural linewidth. However, these works may inspire how to obtain the SPS with subnatural and even ultranarrow linewidth.

Further, we explore whether it is possible by means of the design of physical mechanism, to focus all the spectral components of fluorescent single photon on a bandwidth much smaller than the intrinsic natural linewidth of emitter, and even realize the artificial manipulation of the linewidth of single photon. Specifically, we mainly consider a  $\Lambda$ -shape three-level system as the quantum emitter as shown in Fig. 1(a). The transition from the ground state  $|g\rangle$  to the excited state  $|e\rangle$  is driven by a laser field and the transition between the two ground states  $|g\rangle$  and  $|a\rangle$  is driven by another coherent field. The fluorescence is collected by a detection setup before which a filter with a finite bandwidth is inserted [24, 25]. We find that almost all the spectral components of fluorescence emitted from the transition  $|e\rangle \rightarrow |a\rangle$  can be focused on a bandwidth which is much smaller the natural linewidth of emitter and can be manipulated easily by the coherent fields applied. This complete spectral narrowing effect originates from a specific electron shelving process which dominates the emission of the fluorescence concerned. Therefore, an excellent single-photon response can always arise when the bandwidth of target is approaching and even much smaller than the natural linewidth of emitter, which verifies the realization of the SPS with an ultranarrow linewidth. The experimental feasibility of the scheme proposed here can be demonstrated based on real physical systems.

*Theoretical Model.* Experiments based on the resonance fluorescence of the two-level system demonstrate that the single-photon character and subnatural linewidth cannot simultaneously be observed in simple resonant excitation [24, 25]. As mentioned above, the main purpose of this work is to explore the SPS scheme beyond the limitation of the intrinsic natural linewidth

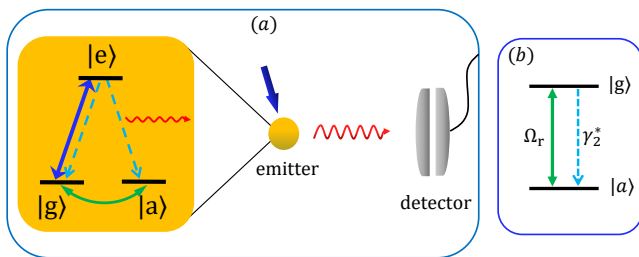


FIG. 1. (Color online) (a) Schematic diagram of the emitter and detector. The emitter is a  $\Lambda$ -shape system including ground states  $|g\rangle$  and  $|a\rangle$ , and excited state  $|e\rangle$ . The fluorescent photon from the transition  $|e\rangle \rightarrow |a\rangle$  is collected by a generalized detection setup. (b) Schematic diagram of the equivalent two-level system of the emitter in (a) in the weak excitation regime.

of emitter. For this purpose, the principle of SPS with a bandwidth much smaller than the natural linewidth of the emitter is demonstrated.

As shown in Fig. 1(a), a  $\Lambda$ -shape system is considered as the quantum emitter, where the transition  $|g\rangle \leftrightarrow |e\rangle$  is driven by a laser field, and the transition  $|g\rangle \leftrightarrow |a\rangle$  is driven by another coherent field (a DC field is applied for simplicity). At the same time, the fluorescence radiated by the emitter is collected by a generalized detector, which can be a detection setup or other optical target, e.g., filter, HBT and HOM setups, and is collectively called detector in the rest of the paper to facilitate the following discussion. We follow an alternative theory formalism adopted in Ref. [38], where the detector is included in the theoretical model and modeled by a quantized harmonic oscillator with bosonic annihilation operator  $s$ . Therefore, the Hamiltonian of the system is given by  $H_{Th} = \Delta_e \sigma_{ee} + \Delta_s s^\dagger s + (\Omega \sigma_{eg} + \Omega_r \sigma_{ga} + g \sigma_{ea} s + H.c)$  in the frame rotating at the laser frequency  $\omega_L$ . Here  $\Delta_p = \omega_p - \omega_L$  ( $p=e, s$ ) represents the frequency detuning between the emitter (or detector) and the laser, and we set  $\Delta_p = 0$  for simplify.  $\Omega$  and  $\Omega_r$  respectively represent the Rabi frequencies of the laser and DC field.  $g$  is the coupling coefficient between the detector and the detected transition  $|e\rangle \rightarrow |a\rangle$ . Therefore, the evolution of the combined system composed of the emitter and detector is governed by the master equation  $\dot{\rho} = -i[H_{Th}, \rho] + \gamma_1 D[\sigma_{ge}]\rho + \gamma_2 D[\sigma_{ae}]\rho + \kappa D[s]\rho$ , where  $D[o]\rho \equiv o\rho o^\dagger - \frac{1}{2}\rho o^\dagger o - \frac{1}{2}o^\dagger o\rho$  is the Lindblad superoperator.  $\gamma_1$  and  $\gamma_2$  respectively represent the decay rates from the excited  $|e\rangle$  to the ground states  $|g\rangle$  and  $|a\rangle$ . The detection bandwidth  $\kappa$  and its inverse, respectively, reflect the frequency and time resolutions of detector, therefore, the constraints imposed by the uncertainty principle on the detection process are included in a self-consistent way.

*Equivalent Level System.* In the limit of the vanishing coupling between the emitter and detector, i.e.,  $g \rightarrow 0$ , the detector can be regarded as a passive ob-

ject [38, 39]. Therefore, it is beneficial to study the nature of the emitter before considering the detection response for this quantum source. In the weak excitation regime of the emitter, i.e.,  $\Omega, \Omega_r \ll \gamma_1, \gamma_2$ , the evolution rate of the excited state is much greater than that of the ground states. Therefore, the excited state can be adiabatically eliminated, which induces equivalent dissipations in the degrees of freedom of the ground states, i.e.,  $\mathcal{L}_{eff}\rho_g = \gamma_1^* D[\sigma_{gg}]\rho_g + \gamma_2^* D[\sigma_{ag}]\rho_g$ . The first term denotes the dephasing of the state  $|g\rangle$ , and the second term denotes the equivalent decay  $|g\rangle \rightarrow |a\rangle$ . The equivalent decay rates satisfy  $\gamma_i^* = \frac{4\gamma_i|\Omega|^2}{(\gamma_1 + \gamma_2)^2}$  ( $i=1,2$ ), which can be reduced to  $\gamma^* = \frac{|\Omega|^2}{\gamma}$  when  $\gamma_1 = \gamma_2 = \gamma$ .

Therefore, the emitter in Fig. 1(a) can be equivalent to a two-level system driven by a coherent field as shown in Fig. 1(b). The equivalent decay  $|g\rangle \rightarrow |a\rangle$  corresponds to a two-photon process in the original level system where the emitter absorbs the first photon by the transition  $|g\rangle \leftrightarrow |e\rangle$  driven by the laser, and subsequently emits the second photon by the spontaneous decay  $|e\rangle \rightarrow |a\rangle$ . Remarkably, different from the conventional two-level system, the decay rate of the equivalent two-level system is determined by the ratio of the intensity of laser to the natural linewidth of emitter and therefore can be set artificially, which may have potential applications in extensive quantum technology fields.

*Spectral Property of Fluorescent Photon.* The intensity of fluorescence from the transition  $|e\rangle \rightarrow |a\rangle$  in the steady-state limit is determined by the steady-state population of excited state  $\langle \sigma_{ee} \rangle = \frac{2\Omega^2\Omega_r^2}{\Omega^4 + 2\Omega_r^2(2\gamma^2 + \Omega^2 + 2\Omega_r^2)}$ , and the corresponding fluorescence spectrum is described by  $S_{ea}(\omega) = Re \int_0^\infty d\tau \lim_{t \rightarrow \infty} \langle \sigma_{ea}(t) \sigma_{ae}(t + \tau) \rangle e^{i\omega\tau}$ .

One can see from Figs. 2(a) and (b) that different spectral structures exhibit for different Rabi frequency  $\Omega_r$ , which can be understood by means of the equivalent two-level system shown in Fig. 1(b). As mentioned above, the equivalent decay  $|g\rangle \rightarrow |a\rangle$  corresponds to the two-photon process composed of the transition  $|g\rangle \leftrightarrow |e\rangle$  driven by laser and the spontaneous decay  $|e\rangle \rightarrow |a\rangle$ . It can be seen that the parameters adopted in Fig. 2(a) correspond to the weak excitation regime in the equivalent two-level system, i.e.,  $\Omega_r \ll \gamma^*$ . Therefore, the fluorescence spectrum of the equivalent decay  $|g\rangle \rightarrow |a\rangle$  exhibits a single-peak structure, whose linewidth is determined by the equivalent decay rate  $\gamma^*$ . And since the laser frequency is constant, the transition  $|e\rangle \rightarrow |a\rangle$  exhibits the same spectral structure as that in the equivalent decay  $|g\rangle \rightarrow |a\rangle$  (see the Supplemental Material [40] for details).

Similarly, the parameters adopted in Fig. 2(b) correspond to the strong excitation regime in the equivalent two-level system, i.e.,  $\Omega_r \gg \gamma^*$ . Therefore, the fluorescence spectrum of the equivalent decay  $|g\rangle \rightarrow |a\rangle$  exhibits a Mollow-like triplet [41, 42], where the spectral widths of the three peaks depend on the equivalent decay

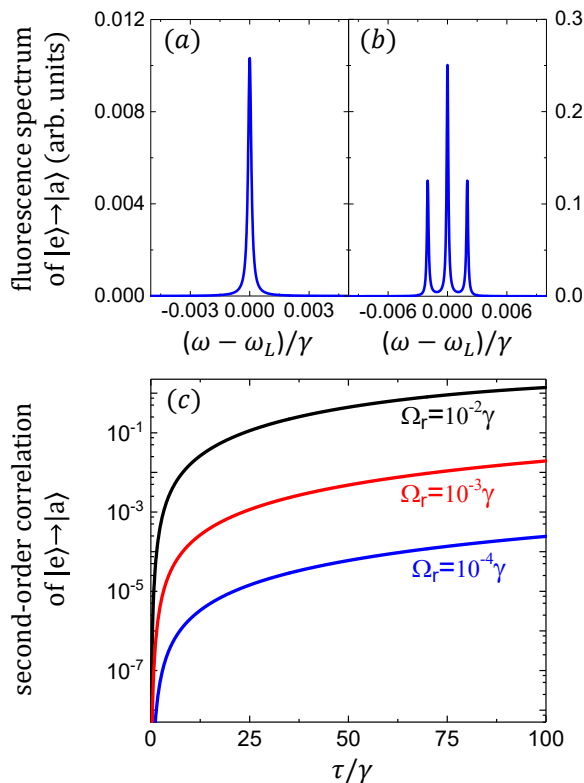


FIG. 2. (Color online) Fluorescence spectrum for the transition  $|e\rangle \leftrightarrow |a\rangle$  is plotted for  $\Omega_r = 10^{-5}\gamma$  and  $10^{-3}\gamma$  (we set  $\gamma_1 = \gamma_2 = \gamma$ ) in (a) and (b), respectively, with other parameter  $\Omega = 10^{-2}\gamma$ . (b) Normalized second-order correlations of the transition  $|e\rangle \rightarrow |a\rangle$  as a function of delay  $\tau$  for  $\Omega = 10^{-2}\gamma$  with different  $\Omega_r$ .

rate  $\gamma^*$  and the positions of the two side peaks depend on the Rabi frequency  $\Omega_r$ . Accordingly, the transition  $|e\rangle \rightarrow |a\rangle$  in the original three-level system exhibits the same Mollow-like triplet (see Supplemental Material [40] for details). Anyhow, all of the fluorescent components are almost focused on a bandwidth of about  $10\gamma^* + 4\Omega_r$  (the proof is in Supplemental Material [40]), which is much smaller than the natural linewidth of emitter. In fact, as long as reducing the intensities of the two external fields, the linewidth of the fluorescent single photon can be narrowed arbitrarily.

For a further insight of the origin of the ultranarrow spectral structure, we next provide an analysis of the fluorescence from another aspect. According to the motion equation of emitter, one can infer that there exists a transition path

$$|g\rangle \leftrightarrow |e\rangle \xrightarrow{\text{decay}} |a\rangle \leftrightarrow |g\rangle, \quad (1)$$

which dominates the emission from the spontaneous decay  $|e\rangle \rightarrow |a\rangle$ . Concretely, the emitter initially in the ground state  $|g\rangle$  is driven to the excited state  $|e\rangle$  by the laser field, and subsequently, the spontaneous decay  $|e\rangle \rightarrow |a\rangle$  takes place. Then, the emitter can only return

to the initial state  $|g\rangle$  by the transition  $|a\rangle \leftrightarrow |g\rangle$  driven by the DC field, and the rate depends on  $\Omega_r$ . Since  $\Omega_r$  is much smaller than the spontaneous decay rate  $\gamma_2$  of the excited state, the system can stay in the state  $|a\rangle$  for a time much longer than the lifetime of emitter, and thus the state  $|a\rangle$  is regarded as the metastable state or the so-called shelving state [6, 43–45]. Consequently, this shelving effect leads to the spectral narrowing of the fluorescence appearing here [34, 35, 45–47]. Further, almost all spectral components of the fluorescence can be concentrated on an ultranarrow bandwidth in the scheme proposed here, and thus the statistical property of fluorescent photon is preserved in this bandwidth, which can be confirmed in following discussions.

*Statistical Property of Fluorescent Photon.* The statistical property of the fluorescence emitted by the transition  $|e\rangle \rightarrow |a\rangle$  can be reflected by the normalized second-order correlation  $g_{ea}^{(2)}(\tau) = \lim_{t \rightarrow \infty} \frac{\langle \sigma_{ea}(t)\sigma_{ea}(t+\tau)\sigma_{ae}(t+\tau)\sigma_{ae}(t) \rangle}{\langle \sigma_{ee}(t) \rangle^2}$  as shown in Fig. 2(c). One see that the correlation  $g_{ea}^{(2)}(\tau)$  remains a value very close to zero even when the delay  $\tau$  is far larger than the lifetime of emitter. Only when the delay reaches to the degree comparable to the inverse of the Rabi frequency  $\Omega_r$ , can the correlation  $g_{ea}^{(2)}(\tau)$  deviates significantly from zero. The above feature of the correlation function can be understood according to the transition path shown in Eq. (1). The emitter is driven from the ground state  $|g\rangle$  to the excited state  $|e\rangle$ , and then enters into the metastable state  $|a\rangle$  after emitting the first photon from the spontaneous decay  $|e\rangle \rightarrow |a\rangle$ . The transitions involved can be equivalent to a decay in the equivalent two-level system, and the corresponding rate is determined by the equivalent decay rate  $\gamma^*$ . After a long time determined by  $\Omega_r$ , the emitter is driven from the metastable state  $|a\rangle$  to the initial state  $|g\rangle$ . Subsequently, the system can be excited again by the laser and then emit the second target photon. Consequently, it is understandable that the correlation function  $g_{ea}^{(2)}(\tau)$  remains zero for a long delay whose length is determined by the equivalent decay rate  $\gamma^*$  and the Rabi frequency  $\Omega_r$  (the proof is in Supplemental Material [40]).

*Detection Response.* Single-photon character is the global property of fluorescence including all spectral components. And, according to Ref. [24, 25], only when the detector (or filter) bandwidth is much larger than the linewidth of fluorescent photon so that the dominant fluorescent components are included, can single-photon character be maintained when detected. Therefore, to test whether the SPS with a linewidth much smaller than the natural linewidth of emitter is obtained successfully, we consider the response of single photon on the detector with a certain bandwidth, which can be described by the

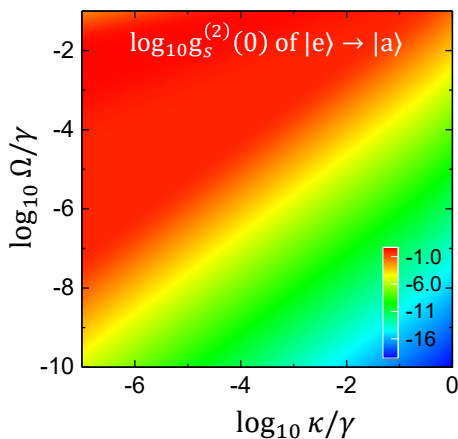


FIG. 3. (Color online) Normalized two-photon correlations of the detector for the transition  $|e\rangle \rightarrow |a\rangle$  as a function of detection bandwidth  $\kappa$  and interaction energy of coherent fields with  $\Omega_r = \Omega$ .

zero delay two-photon correlation [38]

$$g_s^{(2)}(0) = \lim_{t \rightarrow \infty} \frac{\langle s^\dagger(t) s^\dagger(t) s(t) s(t) \rangle}{\langle s^\dagger(t) s(t) \rangle^2}. \quad (2)$$

We show the correlation  $g_s^{(2)}(0)$  as a function of the detection bandwidth and the intensities of the external fields in Fig. 3. It can be demonstrated that when the detection bandwidth is approaching the natural linewidth of the emitter, an excellent single-photon response for the single-photon emission is realized on the detector. According to the earlier discussion on the spectral and statistical properties of the resonance fluorescence of emitter, the physical origin of the excellent single-photon response on the detector can be understood. In terms of frequency, we know that in the weak excitation regime, almost all the spectral components of fluorescence are concentrated on a bandwidth which is much smaller than the natural linewidth of the emitter. Therefore, when filtered by a detection bandwidth approaching the natural linewidth of emitter, all spectral components of the fluorescence are proportionally responded to by the detector, and thus the perfect single-photon character of the fluorescence is preserved well. In turn, the excellent single-photon response for the quantum source on the detector can also confirm the previous conclusion that the dominant components of fluorescence are concentrated on a bandwidth much smaller than the natural linewidth of emitter.

The above discussion can be consistent with the analyse in terms of time. After a photon is emitted from the transition  $|e\rangle \rightarrow |a\rangle$ , the long period of the transition path shown in Eq. (1) leads to that the reemission of the photon from the same decay channel requires a long average time, which is determined by the equivalent decay rate  $\gamma^*$  and the Rabi frequency  $\Omega_r$ . When the detection

bandwidth is approaching the natural linewidth of emitter, the indeterminacy in the time resolution of detection ( $1/\kappa$ ) is approaching the natural lifetime of emitter. Within this indeterminacy, the normalized probability of reemission is very close to zero as shown in Fig. 2(c), and an excellent single-photon response arises on the detector.

Besides, one can see in Fig. 3 that even if the detector bandwidth is much smaller than the natural linewidth of the emitter, i.e.,  $\kappa \ll \gamma$ , the excellent single-photon response on the detector can still be maintained by means of the manipulation of the external fields. Therefore, it can be concluded that the SPS with an ultranarrow linewidth is achieved. Moreover, the linewidth of SPS can be manipulated easily by adjusting the intensities of external coherent fields, which dramatically facilitates the experimental implementation of the narrowing SPS scheme described here.

*Discussion of experimental feasibility.* The experimental progresses on quantum information technology based on the single  $^{87}\text{Rb}$  atom loaded into an optical dipole trap are reported [48–50], which provide a promising candidate of quantum node for implementing quantum repeater and quantum network. One know it is a critical capability for a quantum node to generate high-quality quantum source, therefore the implementation of the ultranarrow SPS scheme proposed here based on the above experimental schemes will be of interest. Specifically, the closed hyperfine transition  $F_g = 1 \rightarrow F_e = 0$  of the  $D_2$  line of  $^{87}\text{Rb}$  is driven by a circularly polarized light resonantly and the transitions between the ground-state Zeeman sublevels are driven by the magnetic field perpendicular to the direction of light propagation simultaneously, so that the narrowing SPS scheme can be achieved (see Supplemental Material [40] for more details). In this scheme, the coherent transition between the ground-state Zeeman sublevels can also be realized by a stimulated Raman transition alternatively. In addition, the SPS scheme can also be implemented based on the  $\Lambda$ -level structure contained in the charged GaAs and InGaAs quantum dots in Voigt magnetic field [51, 52], where a transition between an electron-spin ground state ( $|\uparrow\rangle$  or  $|\downarrow\rangle$ ) and trion excited state ( $|\downarrow\uparrow\uparrow\rangle$  or  $|\downarrow\uparrow\downarrow\rangle$ ) can be driven by a laser resonantly, and the coherent transition between electron-spin ground states can be realized by magnetic field or stimulated Raman process. And as mentioned in Refs. [24, 25], the corresponding detection of two-photon correlation of the fluorescence can be implemented in experiments by inserting a spectral filter with a certain bandwidth in the detection path.

*Conclusion.* We propose the scheme of SPS with a linewidth much smaller than the natural linewidth of emitter under the premise of inheriting the perfect single-photon character of fluorescence, and the single-photon linewidth can be manipulated by coherent fields easily. The above property of fluorescence originates from a spe-

cific electron shelving process which dominates the emission of fluorescence. Accordingly, an excellent single-photon response for the single-photon emission can arise on detector when the detection bandwidth is approaching and even much smaller than the natural linewidth of emitter, which verifies the realization of SPS with ultranarrow linewidth.

It is worth noting that since the perfect single-photon character and ultranarrow linewidth are simultaneously realized when the fluorescent photon is emitted, any additional source or manipulation is no need for these purposes. Therefore, the SPS scheme proposed here is applicable to the quantum information fields. For instance, this scheme can avoid the single photon as the flying qubit carrying information is “polluted”, therefore, the potential security loopholes in quantum communication can be avoided. Although the generation mechanism and experimental feasibility of the SPS with ultranarrow linewidth are our main focus here, further researches based on this work, e.g., the on-demand SPS scheme and the experimental implementations, are worth expecting.

This work is supported by the National Natural Science Foundation of China (Grants No. 11774118 and No. 11474119) and the Fundamental Research Funds for the Central Universities of MOE (Grants No. CCNU18CXTD01 and No. CCNU17TS0006). H.-B. Z. would like to thank Jizhou Wu for valuable discussions.

---

\* zhanghbqm@163.com

† gaox@mail.ccnu.edu.cn

- [1] J. L. O’Brien, *Science* **318**, 1567 (2007).
- [2] J. L. O’Brien, A. Furusawa, and J. Vučković, *Nature Photonics* **3**, 687 (2009).
- [3] H. J. Kimble, M. Dagenais, and L. Mandel, *Phys. Rev. Lett.* **39**, 691 (1977).
- [4] P. Grangier, G. Roger, A. Aspect, A. Heidmann, and S. Reynaud, *Phys. Rev. Lett.* **57**, 687 (1986).
- [5] G. Rempe, F. Schmidt-Kaler, and H. Walther, *Phys. Rev. Lett.* **64**, 2783 (1990).
- [6] J. C. Bergquist, R. G. Hulet, W. M. Itano, and D. J. Wineland, *Phys. Rev. Lett.* **57**, 1699 (1986).
- [7] M. Schubert, I. Siemers, R. Blatt, W. Neuhauser, and P. E. Toschek, *Phys. Rev. Lett.* **68**, 3016 (1992).
- [8] P. Michler, A. Kiraz, C. Becher, W. V. Schoenfeld, P. M. Petroff, L. Zhang, E. Hu, and A. Imamoglu, *Science* **290**, 2282 (2000).
- [9] C. Santori, D. Fattal, J. Vučković, G. S. Solomon, and Y. Yamamoto, *Nature* **419**, 594 (2002).
- [10] Z. Yuan, B. E. Kardynal, R. M. Stevenson, A. J. Shields, C. J. Lobo, K. Cooper, N. S. Beattie, D. A. Ritchie, and M. Pepper, *Science* **295**, 102 (2002).
- [11] B. D. Gerardot, S. Strauf, M. J. A. de Dood, A. M. Bychkov, A. Badolato, K. Hennessy, E. L. Hu, D. Bouwmeester, and P. M. Petroff, *Phys. Rev. Lett.* **95**, 137403 (2005).
- [12] C. Kurtsiefer, S. Mayer, P. Zarda, and H. Weinfurter, *Phys. Rev. Lett.* **85**, 290 (2000).
- [13] Y.-M. He, Y. He, Y.-J. Wei, D. Wu, M. Atatüre, C. Schneider, S. Höfling, M. Kamp, C.-Y. Lu, and J.-W. Pan, *Nature Nanotechnology* **8**, 213 (2013).
- [14] X. Ding, Y. He, Z.-C. Duan, N. Gregersen, M.-C. Chen, S. Unsleber, S. Maier, C. Schneider, M. Kamp, S. Höfling, C.-Y. Lu, and J.-W. Pan, *Phys. Rev. Lett.* **116**, 020401 (2016).
- [15] L. M. Duan, M. D. Lukin, J. I. Cirac, and P. Zoller, *Nature* **414**, 413 (2001).
- [16] E. Knill, R. Laflamme, and G. J. Milburn, *Nature* **409**, 46 (2001).
- [17] P. Kok, W. J. Munro, K. Nemoto, T. C. Ralph, J. P. Dowling, and G. J. Milburn, *Rev. Mod. Phys.* **79**, 135 (2007).
- [18] W. Yao, R.-B. Liu, and L. J. Sham, *Phys. Rev. Lett.* **95**, 030504 (2005).
- [19] H. J. Kimble, *Nature* **453**, 1023 (2008).
- [20] J.-W. Pan, Z.-B. Chen, C.-Y. Lu, H. Weinfurter, A. Zeilinger, and M. Żukowski, *Rev. Mod. Phys.* **84**, 777 (2012).
- [21] N. Somaschi, V. Giesz, L. De Santis, J. C. Loredó, M. P. Almeida, G. Hornecker, S. L. Portalupi, T. Grange, C. Antón, J. Demory, C. Gómez, I. Sagnes, N. D. Lanzillotti-Kimura, A. Lemaître, A. Auffeves, A. G. White, L. Lanco, and P. Senellart, *Nature Photonics* **10**, 340 (2016).
- [22] F. Liu, A. J. Brash, J. O’Hara, L. M. P. P. Martins, C. L. Phillips, R. J. Coles, B. Royall, E. Clarke, C. Bentham, N. Prtljaga, I. E. Itskevich, L. R. Wilson, M. S. Skolnick, and A. M. Fox, *Nature Nanotechnology* **13**, 835 (2018).
- [23] L. Dusanowski, S.-H. Kwon, C. Schneider, and S. Höfling, *Phys. Rev. Lett.* **122**, 173602 (2019).
- [24] L. Hanschke, L. Schweickert, J. C. L. Carreño, E. Schöll, K. D. Zeuner, T. Lettner, E. Z. Casalengua, M. Reindl, S. F. C. da Silva, R. Trotta, J. J. Finley, A. Rastelli, E. del Valle, F. P. Laussy, V. Zwiller, K. Müller, and K. D. Jöns, *Phys. Rev. Lett.* **125**, 170402 (2020).
- [25] C. L. Phillips, A. J. Brash, D. P. S. McCutcheon, J. Iles-Smith, E. Clarke, B. Royall, M. S. Skolnick, A. M. Fox, and A. Nazir, *Phys. Rev. Lett.* **125**, 043603 (2020).
- [26] M. Kiffner, M. Macovei, J. Evers, and C. H. Keitel, *Progress in Optics* **55**, 85 (2010).
- [27] H. J. Carmichael, A. S. Lane, and D. F. Walls, *Phys. Rev. Lett.* **58**, 2539 (1987).
- [28] C. H. Keitel, P. L. Knight, L. M. Narducci, and M. O. Scully, *Optics Communications* **118**, 143 (1995).
- [29] P. Zhou and S. Swain, *Phys. Rev. Lett.* **77**, 3995 (1996).
- [30] P. Zhou and S. Swain, *Phys. Rev. A* **56**, 3011 (1997).
- [31] M. Kiffner, J. Evers, and C. H. Keitel, *Phys. Rev. Lett.* **96**, 100403 (2006).
- [32] M. Kiffner, J. Evers, and C. H. Keitel, *Phys. Rev. A* **73**, 063814 (2006).
- [33] J. Evers, D. Bullock, and C. H. Keitel, *Optics Communications* **209**, 173 (2002).
- [34] B. M. Garraway, M. S. Kim, and P. L. Knight, *Optics Communications* **117**, 560 (1995).
- [35] G. C. Hegerfeldt and M. B. Plenio, *Phys. Rev. A* **52**, 3333 (1995).
- [36] L. M. Narducci, M. O. Scully, G.-L. Oppo, P. Ru, and J. R. Tredicce, *Phys. Rev. A* **42**, 1630 (1990).
- [37] A. S. Manka, H. M. Doss, L. M. Narducci, P. Ru, and G.-L. Oppo, *Phys. Rev. A* **43**, 3748 (1991).
- [38] E. del Valle, A. Gonzalez-Tudela, F. P. Laussy, C. Tejedor,

- dor, and M. J. Hartmann, *Phys. Rev. Lett.* **109**, 183601 (2012).
- [39] J. L. Carreño, E. Z. Casalengua, F. P. Laussy, and E. del Valle, *Quantum Science and Technology* **3**, 045001 (2018).
- [40] See the Supplemental Material at H.-b. Zhang and G.-x. Li, for the analytical results and corresponding discussions about the steady-state density operator, fluorescence spectrum and second-order correlation of the emitter, and example implementation of the SPS scheme based on real physical systems, which includes Refs.[41, 42, 48-50]
- [41] B. R. Mollow, *Phys. Rev.* **188**, 1969 (1969).
- [42] F. Y. Wu, R. E. Grove, and S. Ezekiel, *Phys. Rev. Lett.* **35**, 1426 (1975).
- [43] W. Nagourney, J. Sandberg, and H. Dehmelt, *Phys. Rev. Lett.* **56**, 2797 (1986).
- [44] T. Sauter, W. Neuhauser, R. Blatt, and P. E. Toschek, *Phys. Rev. Lett.* **57**, 1696 (1986).
- [45] M. B. Plenio and P. L. Knight, *Rev. Mod. Phys.* **70**, 101 (1998).
- [46] J. Evers and C. H. Keitel, *Phys. Rev. A* **65**, 033813 (2002).
- [47] V. Bühner and C. Tamm, *Phys. Rev. A* **61**, 061801 (2000).
- [48] J. Volz, M. Weber, D. Schlenk, W. Rosenfeld, J. Vrana, K. Saucke, C. Kurtsiefer, and H. Weinfurter, *Phys. Rev. Lett.* **96**, 030404 (2006).
- [49] J. Hofmann, M. Krug, N. Ortegel, L. Gérard, M. Weber, W. Rosenfeld, and H. Weinfurter, *Science* **337**, 72 (2012).
- [50] T. van Leent, M. Bock, R. Garthoff, K. Redeker, W. Zhang, T. Bauer, W. Rosenfeld, C. Becher, and H. Weinfurter, *Phys. Rev. Lett.* **124**, 010510 (2020).
- [51] M. V. G. Dutt, J. Cheng, B. Li, X. Xu, X. Li, P. R. Berman, D. G. Steel, A. S. Bracker, D. Gammon, S. E. Economou, R.-B. Liu, and L. J. Sham, *Phys. Rev. Lett.* **94**, 227403 (2005).
- [52] Y. He, Y.-M. He, Y.-J. Wei, X. Jiang, M.-C. Chen, F.-L. Xiong, Y. Zhao, C. Schneider, M. Kamp, S. Höfling, C.-Y. Lu, and J.-W. Pan, *Phys. Rev. Lett.* **111**, 237403 (2013).

# Supplemental Material for “Single-photon source with ultranarrow linewidth manipulated by coherent fields”

He-bin Zhang<sup>1,\*</sup> and Gao-xiang Li<sup>1,†</sup>

<sup>1</sup>*Department of Physics, Huazhong Normal University, Wuhan 430079, China*

(Dated: December 24, 2024)

arXiv:2103.11801v1 [quant-ph] 22 Mar 2021

## Abstract

This supplementary material contains two parts: I. The steady-state solution of the emitter shown in Fig.1 of the main text is given and discussed. Besides, the analytical expressions of the fluorescence spectrum and second-order correlation of the transition  $|e\rangle \rightarrow |a\rangle$  are given, and some points involved in the main text are proved analytically. II. We choose the closed transition  $F_g = 1 \rightarrow F_e = 0$  of the  $D_2$  line of  $^{87}\text{Rb}$  as the emitter to demonstrate the experimental feasibility of the SPS scheme proposed in the main text. In addition, some other realization candidates based on the alkali-metal atom systems are discussed.

## GENERAL SOLUTION FOR EMITTER SYSTEM

### Steady-state solution of density matrix

As mentioned in the main text, in the limit of the vanishing coupling between the emitter and detector, the detector can be regarded as a passive object and does not cause backaction on the emitter. Therefore, we can separately solve and discuss the part of the motion equation describing the evolution of the emitter, that is,

$$\dot{\rho}_\sigma = -i[H_A, \rho_\sigma] + \gamma_1 D[\sigma_{ge}] \rho_\sigma + \gamma_2 D[\sigma_{ae}] \rho_\sigma, \quad (1)$$

where  $H_A = \Omega\sigma_{eg} + \Omega_r\sigma_{ga} + H.c$  is the Hamiltonian of the emitter, and  $\rho_\sigma$  represents the reduced density matrix of the emitter. And under steady-state conditions, we get the analytical solutions of the density matrix elements of the emitter

$$\begin{aligned} \rho_{gg} &= \frac{\Omega_r^2(2\gamma^2 + \Omega^2 + 2\Omega_r^2)}{M}, \\ \rho_{aa} &= \frac{\Omega^4 + \Omega_r^2(2\gamma^2 - \Omega^2 + 2\Omega_r^2)}{M}, \\ \rho_{ee} &= \frac{2\Omega^2\Omega_r^2}{M}, \\ \rho_{ge} &= \frac{2i\gamma\Omega\Omega_r^2}{M}, \\ \rho_{ae} &= \frac{-\Omega^3\Omega_r + 2\Omega\Omega_r^3}{M}, \\ \rho_{ga} &= \frac{-i\gamma\Omega^2\Omega_r}{M}, \end{aligned} \quad (2)$$

where  $M = \Omega^4 + 2\Omega_r^2(2\gamma^2 + \Omega^2 + 2\Omega_r^2)$  (we assume  $\gamma_1 = \gamma_2 = \gamma$  for simplicity). It can be seen that when the DC field is removed, the state  $|a\rangle$  become a dark state on which all the populations are focused.



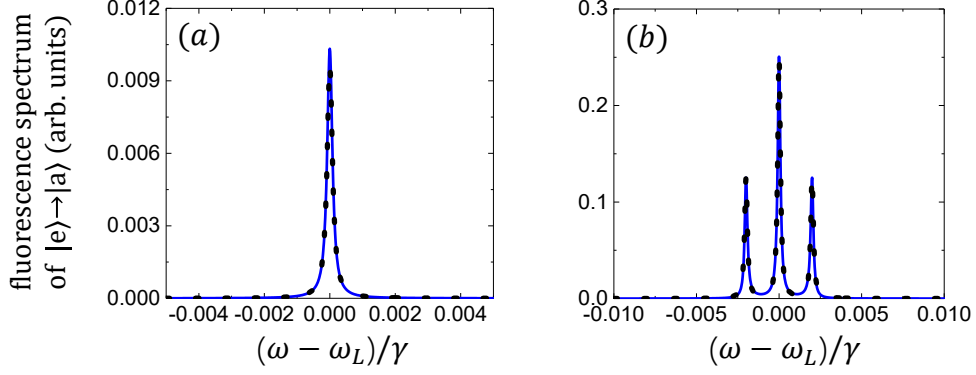


FIG. 1. (Color online) The analysis results (solid line) of the fluorescence spectrum according to Eqs. (9) and (15) are compared with the numerical results (dotted line) to verify the accuracy of the theory in this section. The parameters applied in (a) and (b) are the same as that in Figs.1(c) and (d).

### Analytical expression of fluorescence spectrum

The steady-state fluorescence spectrum for the transition  $|e\rangle \rightarrow |a\rangle$  in the far-zone is given by

$$S_{ea}(\omega) = Re \int_0^\infty d\tau \lim_{t \rightarrow \infty} \langle \sigma_{ea}(t) \sigma_{ae}(t + \tau) \rangle e^{i\omega\tau}, \quad (3)$$

and can be calculated by means of the quantum regression theorem [1, 2].

In the equivalent weak excitation regime, i.e.,  $\Omega_r \ll \gamma^*$ , the analytical expression of the fluorescence spectrum can be obtained by the perturbation method as

$$S_{ea}^{ew}(\omega) = S_c^{ew}(\omega) + S_n^{ew}(\omega) + S_b^{ew}(\omega). \quad (4)$$

Here  $S_c^{ew}(\omega)$  represents the coherent part of the the fluorescence and is given by

$$S_c^{ew}(\omega) = \gamma |\rho_{ae}|^2 \delta(\omega). \quad (5)$$

$S_n^{ew}(\omega)$  represents the incoherent narrow spectral components of the the fluorescence and is given by

$$S_n^{ew}(\omega) = \frac{-i\rho_{ge}\Omega^2 + \rho_{ae}\gamma\Omega_r}{\Omega} \frac{\gamma^*}{\omega^2 + \gamma^{*2}}, \quad (6)$$

with  $S_b^{ew}(\omega)$  represents the incoherent broad spectral components and is given by

$$S_b^{ew}(\omega) = \rho_{ae}\Omega\Omega_r \frac{1}{\omega^2 + \gamma^2} - \frac{2i\rho_{ge}\Omega^3}{\gamma} \frac{\gamma^2 - \omega^2}{(\gamma^2 + \omega^2)^2}. \quad (7)$$

It can be obtained that the ratio between the total intensities of the broad and narrow spectral components is

$$\frac{\int_{-\infty}^{\infty} d\omega S_b^{ew}}{\int_{-\infty}^{\infty} d\omega S_n^{ew}} = \frac{\Omega^2}{\gamma^2}, \quad (8)$$

which is much less than 1. Therefore, the broad spectral components can be ignored, and the analytical expression of the fluorescence spectrum can be reduced as

$$S_{ea}^{ew}(\omega) = S_c^{ew}(\omega) + S_n^{ew}(\omega), \quad (9)$$

which is in good agreement with the exact numerical result according to Fig. 1(a). We see that the fluorescence spectrum exhibits a single-peak structure whose linewidth is the equivalent decay rate  $\gamma^*$ , which means that the spectral width of the fluorescence can be much smaller than the intrinsic linewidth of emitter  $\gamma$  as shown in Fig. 1(a).

In the equivalent stronger excitation regime, i.e.,  $\Omega_r \gg \gamma^*$ , the analytical expression of the fluorescence spectrum can be obtained as

$$S_{ea}^{es}(\omega) = S_c^{es}(\omega) + S_n^{es}(\omega) + S_b^{es}(\omega). \quad (10)$$

Here  $S_c^{es}(\omega)$  represents the coherent part of the the fluorescence and is given by

$$S_c^{es}(\omega) = \gamma |\rho_{ae}|^2 \delta(\omega). \quad (11)$$

$S_n^{es}(\omega)$  represents the incoherent narrow spectral components of the fluorescence and is given by

$$S_n^{es}(\omega) = -\frac{i}{4} \rho_{ge} \Omega \left( \frac{2\gamma^*}{\omega^2 + \gamma^{*2}} + \frac{\gamma^*}{(\omega - 2\Omega_r)^2 + \gamma^{*2}} + \frac{\gamma^*}{(\omega + 2\Omega_r)^2 + \gamma^{*2}} \right). \quad (12)$$

$S_b^{es}(\omega)$  represents the incoherent broad spectral components and is given by

$$S_b^{es}(\omega) = \rho_{ae} \Omega \Omega_r \frac{1}{\omega^2 + \gamma^2}. \quad (13)$$

It can also be obtained that the ratio between the total intensities of the broad and narrow spectral components is

$$\frac{\int_{-\infty}^{\infty} d\omega S_b^{es}}{\int_{-\infty}^{\infty} d\omega S_n^{es}} = \frac{\Omega^2 - 2\Omega_r^2}{2\gamma^2}, \quad (14)$$

which is far smaller than 1. Therefore, the broad spectral components can be ignored, and the analytical expression of the fluorescence spectrum can be reduced as

$$S_{ea}^{es}(\omega) = S_c^{es}(\omega) + S_n^{es}(\omega), \quad (15)$$

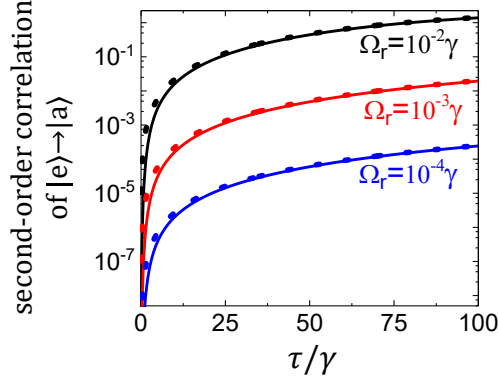


FIG. 2. (Color online) The analysis results (dotted line) of the correlation function according to Eq. (16) are compared with the numerical results (solid line) to verify the accuracy of the theory in this section. The parameters used here are the same as that in Fig.1(e).

which is in good agreement with the exact numerical result according to Fig. 1(b). We see that the fluorescence spectrum exhibits a Mollow-like triplet [3, 4]. The spectral width of each peak also depends on the equivalent decay rate  $\gamma^*$ , thus is much smaller than the natural linewidth of the excited state in the parameter regime concerned here. Moreover, since the two ultranarrow sidebands arise at frequencies  $\omega_L \pm 2\Omega_r$ , one can infer that all the spectral components of fluorescence are concentrated in a bandwidth of  $4\Omega_r$ , which is much smaller than the natural linewidth of emitter as shown in Fig. 1(b).

### Analytical expression of correlation function

In the weak excitation regime, the analytical expression of the normalized second-order correlation  $g_{ea}^{(2)}(\tau)$  can be obtained according to the quantum regression theorem as

$$g_{ea}^{(2)}(\tau) = 1 - \cos(2\Omega_r\tau)e^{-\gamma^*\tau} - \frac{\Omega^2 - 2\Omega_r}{2\gamma\Omega_r} \sin(2\Omega_r\tau)e^{-\gamma^*\tau}, \quad (16)$$

which is in good agreement with the exact numerical result according to Fig. 2. We can see from Eq. (16) that the time evolution of the second-order correlation  $g_{ea}^{(2)}(\tau)$  depends on the equivalent decay rate  $\gamma^*$  and Rabi frequency  $\Omega_r$  of the DC field, both of which are determined by the external coherent fields and thus can be easily manipulated in experiment. In contrast, in the same parameter regime, the second-order correlation function of a normal two-level system (i.e.,  $g_T^{(2)}(\tau) = (1 - e^{-\frac{\gamma_t}{2}\tau})^2$ ) depends entirely on the intrinsic natural linewidth  $\gamma_t$ , which is difficult to modify artificially.

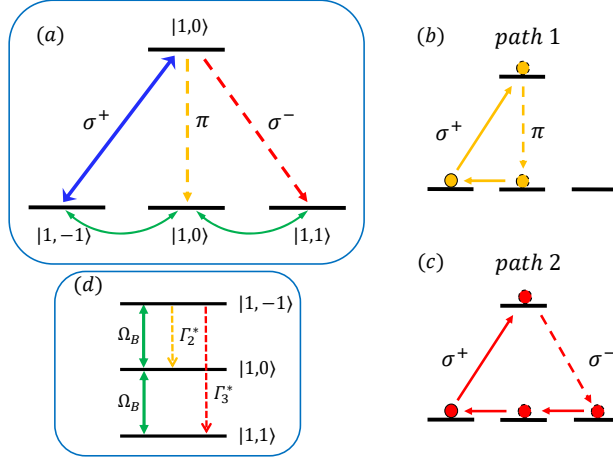


FIG. 3. (Color online) (a) Schematic diagram of the level configuration for the transition  $F_g = 1 \rightarrow F_e = 0$  of the  $D_2$  line of  $^{87}\text{Rb}$ , where the transitions from the ground and excited states and between the ground-state Zeeman sublevels are, respectively, driven by  $\sigma^+$ -polarized laser field ( $\mathbf{E}$ ) and transverse magnetic field ( $\mathbf{B}_T$ ). The transition paths involved in Eqs. (24) and (25) are exhibited in (b) and (c), respectively. (d) Schematic diagram of the equivalent three-level system of the emitter in (a) in the weak excitation regime.

## EXAMPLE IMPLEMENTATION

### Transition $F_g = 1 \rightarrow F_e = 0$ of $D_2$ Line of $^{87}\text{Rb}$

In order to demonstrate the experimental feasibility of SPS scheme proposed on the main text, we choose the closed transition  $F_g = 1 \rightarrow F_e = 0$  of the  $D_2$  line of  $^{87}\text{Rb}$  as the emitter, where  $F_g$  and  $F_e$  respectively represent the total angular momentums of the ground and excited states. And many platforms, e.g., the single  $^{87}\text{Rb}$  atom loaded into an optical dipole trap reported in Refs. [5–7], can be the potential candidates for the scheme implementation. As shown in Fig. 3(a), the ground hyperfine state  $F_g = 1$  is composed of three Zeeman sublevels  $|1, -1\rangle, |1, 0\rangle, |1, 1\rangle$ , and the excited hyperfine state  $F_e = 0$  is composed of one Zeeman sublevel  $|0, 0\rangle$ . The transition  $|1, -1\rangle \leftrightarrow |0, 0\rangle$  is driven by a  $\sigma^+$ -polarized laser field  $\mathbf{E}$ , and we set the quantization axis ( $z$  axis) along the direction propagation of the light beam. We consider a static magnetic field  $\mathbf{B}_T$  perpendicular to the direction of light propagation is applied to drive the transitions between the ground-state Zeeman sublevels, whose direction is set along the  $x$  axis. In spite of the above magneto-optical system, the

transitions between the ground-state Zeeman sublevels can also be replaced by an optical scheme, i.e., stimulated Raman processes in large detuning condition (not shown here). The fluorescence emitted from the excited state to the ground state is collected by a detector, which is modeled by a quantized harmonic oscillator with bosonic annihilation operator  $s$  as in Sec.2 of the main text. In the frame rotating at the laser frequency  $\omega_L$  and within the rotating wave approximation, the Hamiltonian of the combine system composed of the emitter and the detector can be given by

$$H_{Rb} = H_0 + H_I + H_B + H_S. \quad (17)$$

$H_0$  is the nonperturbed Hamiltonian of the emitter

$$H_0 = \Delta_e |F_e, m_e\rangle \langle F_e, m_e| + H.c. \quad (18)$$

where  $\Delta_e$  is the detuning of the transition  $|1, -1\rangle \leftrightarrow |0, 0\rangle$  frequency from the laser.  $H_I$  represents the laser-atom interaction Hamiltonian

$$H_I = \sum_{g_i} V_{eg_i} |F_e, m_e\rangle \langle F_g, m_{g_i}| + H.c. \quad (19)$$

According to the Wigner-Eckart theorem [8–10], the interaction energy for the transition  $|F_g, m_{g_i}\rangle \rightarrow |F_e, m_e\rangle$  can be given by

$$V_{eg_i} = -\langle F_e, m_e | \mathbf{d} | F_g, m_{g_i} \rangle \cdot \mathbf{E} = (-1)^{F_e - m_e + 1} \begin{pmatrix} F_e & 1 & F_g \\ -m_e & q & m_{g_i} \end{pmatrix} \Omega_L, \quad (20)$$

where  $\mathbf{d}$  is the electric dipole operator,  $\Omega_L = \langle F_e || \mathbf{d} || F_g \rangle E$  is the Rabi frequency of the light field, and  $q = 0, \pm 1$  denotes the spherical components.  $H_B$  represents the magnetic-atom interaction Hamiltonian

$$H_B = -\mu_B g_F \mathbf{F} \cdot \mathbf{B}_T = \mu_B g_F B_T \sum_{g_i, g_j} \langle F_g, m_{g_i} | \mathbf{F} | F_g, m_{g_j} \rangle \cdot \mathbf{e}_x |F_g, m_{g_i}\rangle \langle F_g, m_{g_j}|, \quad (21)$$

where  $\mu_B$  and  $g_F$  denote the Bohr magneton and the gyromagnetic factor of the ground states, respectively. And

$$\langle F_g, m_{g_i} | \mathbf{F} | F_g, m_{g_j} \rangle = \langle F || \mathbf{F} || F \rangle (-1)^{F_g - m_{g_i}} \begin{pmatrix} F_g & 1 & F_g \\ -m_{g_i} & q & m_{g_j} \end{pmatrix}. \quad (22)$$

$H_S$  is the Hamiltonian describing the detector and its coupling with the emitter

$$H_S = \Delta_s s^\dagger s + (g A_d s^\dagger + H.c.), \quad (23)$$

where the operator  $A_d$  is defined as  $A_d \equiv |1, d\rangle \langle 0, 0|$  ( $d = 0, \pm 1$ ), and denotes the atomic transition coupled with the detector.

In the weak excitation regime, i.e.,  $V_{eg-1}, \Omega_B \ll \Gamma$ , we can deduce that there exist two main fluorescence emission paths where the shelving effect similar to that in the transition path in Eq.(1) of the main text can arise, that is, path 1 as shown in Fig. 3(b)

$$|1, -1\rangle \leftrightarrow |0, 0\rangle \xrightarrow{\text{decay}} |1, 0\rangle \leftrightarrow |1, -1\rangle, \quad (24)$$

which dominates the emission from the spontaneous decay  $|0, 0\rangle \rightarrow |1, 0\rangle$ , and path 2 as shown in Fig. 3(c)

$$|1, -1\rangle \leftrightarrow |0, 0\rangle \xrightarrow{\text{decay}} |1, 1\rangle \leftrightarrow |1, 0\rangle \leftrightarrow |1, -1\rangle. \quad (25)$$

which dominates the emission from the spontaneous decay  $|0, 0\rangle \rightarrow |1, 1\rangle$ . In path 1 and 2, because the magnetic field driving the transition between the ground states is weak, the emitter can stay in the states  $|1, 1\rangle$  and  $|1, 0\rangle$  for a long time, and thus these two states are both the shelving states. Therefore, it is expected that the shelving effect similar to the scheme in the main text can emerge in the fluorescence emitted from the spontaneous decays  $|0, 0\rangle \rightarrow |1, 0\rangle$  and  $|0, 0\rangle \rightarrow |1, 1\rangle$ .

On the other hand, similarly to the case in the main text, equivalent dissipations are introduced into the degrees of freedom of the ground states due to the adiabatic elimination of the excited state, i.e.,  $\mathcal{L}_{eff}\rho_{g'} = \sum_{i=-1}^1 \Gamma_i^* D[\sigma_{g_i g_{-1}}] \rho_{g'}$ , where  $\Gamma_i^* = 4\Gamma_i |V_{eg-1}|^2 / \Gamma^2$  is the equivalent decay rate from the states  $|1, -1\rangle$  to  $|1, i\rangle$ . Therefore, the emitter in Fig. 3(a) can be equivalent to a three-level system driven coherently by the magnetic field as shown in Fig. 3(d). And, the equivalent decays  $|1, -1\rangle \rightarrow |1, 0\rangle$  and  $|1, -1\rangle \rightarrow |1, 1\rangle$  correspond to the decays involved in path 1 and 2, respectively.

### Fluorescence Properties and Detection Response

The fluorescence spectrum of the transitions  $|0, 0\rangle \rightarrow |1, 0\rangle$  and  $|0, 0\rangle \rightarrow |1, 1\rangle$  are shown in Figs. 4(a) and (d). Multi-peak structures arise as the case in the main text, which can also be understood by mean of the equivalent level system in Fig. 3(d). Taking transition  $|0, 0\rangle \rightarrow |1, 0\rangle$  as an example, we explain the origin of the spectral structure. As mentioned above, the equivalent decay  $|1, -1\rangle \rightarrow |1, 0\rangle$  shown in Fig. 3(d) corresponds to the two-photon

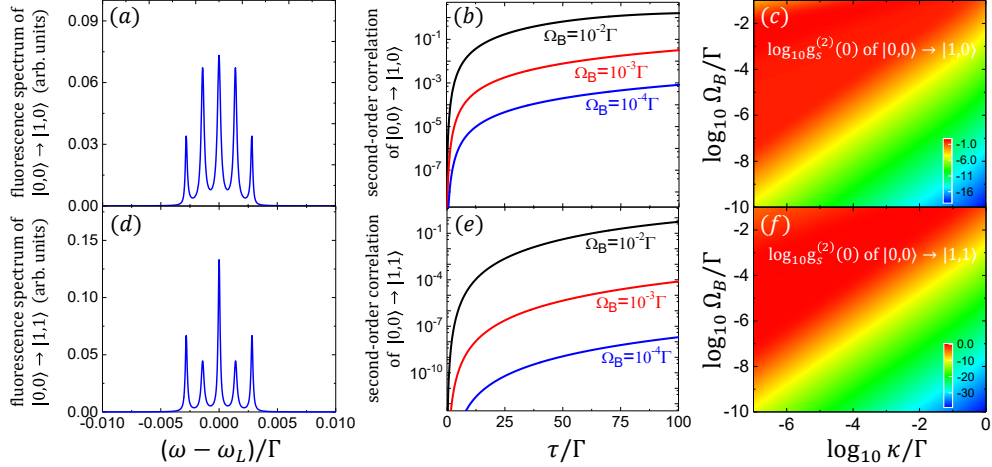


FIG. 4. (Color online) The spectral property, second-ordering correlation and detection response for the fluorescent photon emitted from the transitions  $|0,0\rangle \rightarrow |1,0\rangle$  and  $|0,0\rangle \rightarrow |1,-1\rangle$  are, respectively, exhibited in (a)-(c) and (d)-(f). In (a) and (d), fluorescence spectrum for  $\Omega_B = 10^{-3}\Gamma$  and  $V_{eg-1} = 10^{-2}\Gamma$  ( $\Gamma = 2\pi \times 6.0666\text{MHz}$ ). In (b) and (e), normalized second-ordering correlations as a function of delay  $\tau$  for  $V_{eg-1} = 10^{-2}\Gamma$  with different  $\Omega_B$ . In (c) and (f), normalized two-photon correlations of the detector as a function of detection linewidth  $\kappa$  and the interaction energies of coherent fields with  $\Omega_B = V_{eg-1}$ .

process composed of the transition  $|1,-1\rangle \rightarrow |0,0\rangle$  driven by the laser and the subsequent spontaneous decay  $|0,0\rangle \rightarrow |1,0\rangle$ . According to the standard dressed-state theory, there are four sidebands located at the frequencies  $\pm\sqrt{2}\Omega_B$  and  $\pm 2\sqrt{2}\Omega_B$  in the emission of equivalent decay  $|1,-1\rangle \rightarrow |1,0\rangle$  [11]. And since the laser frequency is constant, the transition  $|0,0\rangle \rightarrow |1,0\rangle$  exhibits the same spectral structure as that in the equivalent decay  $|1,-1\rangle \rightarrow |1,0\rangle$ . Therefore, one can infer that all spectral components of fluorescence are concentrated on a narrow bandwidth about  $4\sqrt{2}\Omega_B$ , which can be much smaller than the natural linewidth of emitter. From another perspective, we can conclude that thanks to the dominant positions of path 1 and path 2 in the formation of the fluorescence from the transitions  $|0,0\rangle \rightarrow |1,0\rangle$  and  $|0,0\rangle \rightarrow |1,1\rangle$ , respectively, the global spectral narrowing caused by the shelving effect similar to the case in the main text can occur in the scheme considered here. In addition, the simple relationship between the sidebands with ultranarrow linewidth and the magnetic field provides the theoretical possibility of the precision measurement of magnetic field.

In Figs. 4(b) and (e), the statistical properties of fluorescence emitted from the transitions

$|0, 0\rangle \rightarrow |1, 0\rangle$  and  $|0, 0\rangle \rightarrow |1, 1\rangle$  are exhibited, respectively. Similarly to the scheme in main text, the normalized second-order correlations of these two transitions can both remain a value very close to zero for a long delay which is much larger than the natural lifetime of the excited state. These features of the correlations confirm that the shelving effects in paths 1 and 2 are, respectively, dominant in the processes emitting the corresponding fluorescence. Moreover, because path 2 has a longer period than path 1, the corresponding second-order correlation can be maintained near zero for a longer time.

According to the above discussion, we see that the nontrivial spectral and statistical properties of the SPS scheme similar to that in the main text can be well realized in the transitions  $|0, 0\rangle \rightarrow |1, 0\rangle$  and  $|0, 0\rangle \rightarrow |1, 1\rangle$  of transition  $F_g = 1 \rightarrow F_e = 0$  of the  $D_2$  line of  $^{87}\text{Rb}$ . Accordingly, the corresponding excellent single-photon responses on the detector with a bandwidth approaching and even much smaller than the natural linewidth of emitter are predicted, which is confirmed in Figs. 4(c) and (f). In addition, because the shelving effect in path 2 is more prominent than that in path 1, the single-photon response for the fluorescent photon from the transition  $|0, 0\rangle \rightarrow |1, 1\rangle$  on the detector is more conspicuous.

### **Other realizable candidates of single-photon emitter**

Besides the closed transition  $F_g = 1 \rightarrow F_e = 0$  of the  $D_2$  line of  $^{87}\text{Rb}$ , the scheme of ultranarrow SPS proposed in the main text can also be implemented in many transition structures based on various alkali-metal atoms, e.g., in other kind of transition  $F_g \rightarrow F_e = F_g, F_g \pm 1$ . Similar to the scheme in the main text, a circularly polarized laser drive resonantly the transitions between the ground and excited states, while a magnetic field perpendicular to the light propagation direction drives the transitions between the ground-state Zeeman sublevels, as shown in Fig. 5.

In the weak excitation regime of the laser and magnetic fields, due to the shelving effect similar to that mentioned in the main text, the SPS with an ultranarrow bandwidth can be realized in the transitions with polarization different from the laser. One can see that the difference between the magnetic quantum numbers of the detected and laser photons is 1 or 2. Therefore, to reload the emitter, the transitions between the ground-state Zeeman sublevels are required, which can be realized easily by the transverse magnetic field. In such schemes of emitter, the single-photon emission is controlled by two external coherent fields,



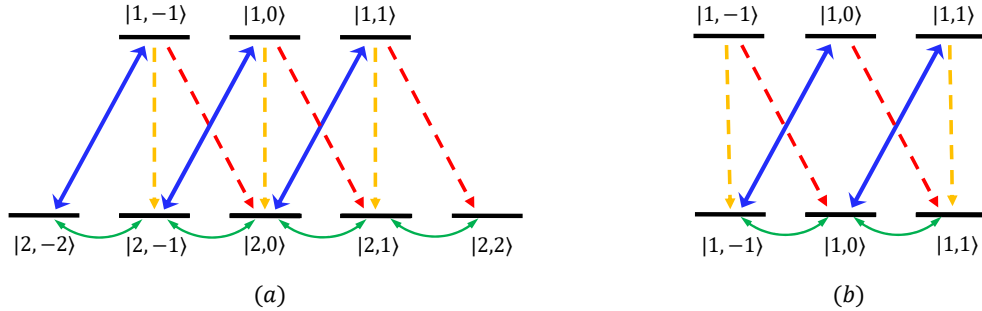


FIG. 5. (Color online) Schematic diagram of the implementation scheme of narrowed single photon source in transitions (a)  $F_g = 2 \rightarrow F_e = 1$  (b)  $F_g = 1 \rightarrow F_e = 1$ . The transitions between the ground states and the excited states are driven by a  $\sigma^+$ -polarized laser field, and photons with multiple polarizations are emitted in spontaneous decays. A transverse magnetic field is applied to drive the transitions between the ground-state Zeeman sublevels (the driving between the excited-state Zeeman sublevels is weak compared to the spontaneous emission process, and thus is ignorable). Choosing the fluorescent photon with a polarization different from the laser as the detection target, the SPS scheme proposed in the main text can be realized.

and thus the linewidth and brightness of the SPS can be manipulated conveniently.

---

\* zhanghbqm@163.com

† gaox@mail.ccnu.edu.cn

- [1] M. Lax, Phys. Rev. **129**, 2342 (1963).
- [2] H. Carmichael, *An Open Systems Approach to Quantum Optics* (Springer, New York, 1993).
- [3] B. R. Mollow, Phys. Rev. **188**, 1969 (1969).
- [4] F. Y. Wu, R. E. Grove, and S. Ezekiel, Phys. Rev. Lett. **35**, 1426 (1975).
- [5] J. Volz, M. Weber, D. Schlenk, W. Rosenfeld, J. Vrana, K. Saucke, C. Kurtsiefer, and H. Weinfurter, Phys. Rev. Lett. **96**, 030404 (2006).
- [6] J. Hofmann, M. Krug, N. Ortegel, L. Gérard, M. Weber, W. Rosenfeld, and H. Weinfurter, Science **337**, 72 (2012).
- [7] T. van Leent, M. Bock, R. Garthoff, K. Redeker, W. Zhang, T. Bauer, W. Rosenfeld, C. Becher, and H. Weinfurter, Phys. Rev. Lett. **124**, 010510 (2020).

- [8] G. K. Woodgate, *Elementary Atomic Structure* (Oxford Scientific, Oxford, 2000).
- [9] D. M. Brink and G. R. Satchler, *Angular Momentum* (Clarendon Press, Oxford, 1994).
- [10] J. L. Meunier, *European Journal of Physics* **8**, 114 (1987).
- [11] H.-b. Zhang, G. Yang, G.-m. Huang, and G.-x. Li, *Physical Review A* **99**, 033803 (2019).